

6-14-2024

## Theoretical study on the insertion reaction of the stannyleneid $H_2SnLiF$ with X-H bonds (X = N, O, F)

SHUO WU

BINGFEI YAN

SHAOLI LIU

WENZUO LI

Follow this and additional works at: <https://journals.tubitak.gov.tr/chem>

 Part of the [Chemistry Commons](#)

### Recommended Citation

WU, SHUO; YAN, BINGFEI; LIU, SHAOLI; and LI, WENZUO (2024) "Theoretical study on the insertion reaction of the stannyleneid  $H_2SnLiF$  with X-H bonds (X = N, O, F)," *Turkish Journal of Chemistry*. Vol. 48: No. 3, Article 4. <https://doi.org/10.55730/1300-0527.3671>  
Available at: <https://journals.tubitak.gov.tr/chem/vol48/iss3/4>



This work is licensed under a [Creative Commons Attribution 4.0 International License](#).

This Research Article is brought to you for free and open access by TÜBİTAK Academic Journals. It has been accepted for inclusion in Turkish Journal of Chemistry by an authorized editor of TÜBİTAK Academic Journals. For more information, please contact [pinar.dundar@tubitak.gov.tr](mailto:pinar.dundar@tubitak.gov.tr).

## Theoretical study on the insertion reaction of the stannylene $H_2SnLiF$ with X-H bonds (X = N, O, F)

Shuo WU<sup>1</sup>, Bingfei YAN<sup>1</sup>, Shaoli LIU<sup>1</sup>, Wenzuo LI\*<sup>1</sup>

Department of Applied Chemistry, School of Chemistry and Chemical Engineering, Yantai University, Yantai, P. R. China

Received: 14.04.2023 • Accepted/Published Online: 02.05.2024 • Final Version: 14.06.2024

**Abstract:** The insertion reactions of p-complex (RP) and three-membered ring configuration (RS) of stannylene  $H_2SnLiF$  with  $NH_3$ ,  $H_2O$  and HF have been studied theoretically by quantum chemical calculation. The structures of reactants, precursors, transition states, intermediates and products have been fully optimized at the M06-2X/def2-TZVP level. The single point energy of all fixed points were calculated using the QCISD method. The calculation results show that the three-membered ring configuration is easier to conduct the insertion reaction. Comparing the reaction energy barriers of RP, RS to  $NH_3$ ,  $H_2O$  and HF, we found that the difficulty of the insertion reaction is  $NH_3 > H_2O > HF$ . The solvent corrected calculation results show that in THF, the reaction energy barrier of RP is lower than that in vacuum, while the reaction energy barrier of RS is higher. This work provides theoretical support for the reaction properties of stannylene.

**Key words:**  $H_2SnLiF$ , X-H, M06-2X, QCISD, insertion reaction

### 1. Introduction

Tetrylenoids  $R_2EXM$  (E = Si, Ge and Sn; X = electronegative group; M = alkali metal) are heavier homologues of carbenoid compounds [1–2], which have electrophilic and nucleophilic properties just like carbenoid. Silylenoids and germylenoids have been successfully synthesized and isolated over decades of exploration, and their structures and reaction properties have been well investigated experimentally and theoretically [3–26]. For example, in 2006, Molev et al. [12] used X-ray crystal diffraction to determine the structure of the first successfully separated fluorolithium silylenoids. From 2010 to 2015, Cho et al. conducted experimental studies on the addition reaction of lithium containing silylenoids with ketones [13], aldehydes [14], and olefins [15]. In terms of theoretical calculations, in 1980, Clark et al. [16] firstly performed theoretical exploration of  $H_2SiLiF$ . In 2014, Qi et al. [17] studied the structural properties of unsaturated silylenoids  $HP = SiLiF$ . In 2016, Yildiz et al. [18] made a theoretical study on the synthesis and rearrangement reaction of cyclic silylenoids. For germylenoids, in 2016, Suzuki et al. [19] synthesized and separated stable chlorine containing germylenoids. In 2007, Ma et al. [20] explored the structure and solvation effect of  $H_2GeLiF$  through theoretical research. Then Li et al. explored the structure and properties of silylenoids containing metal Be [21] and Al [22], respectively. These investigations have promoted people's understanding of the structure and reaction properties of tetralenoids.

Stannylene is a class of tetrylenoids with the structural general formula  $R_1R_2SnXM$ , which is an active intermediate. After decades of research, stannylene has attracted more and more attention in the field of organotin chemistry, and a large number of experimental studies have also been carried out. Grugel [27] team was the first to predict the existence of stannylene compounds in the reaction of aldehyde with some stannylene precursors. Then Arif et al. [28] and Ochiai et al. [29] successfully isolated the stannylene compounds and observed their structures by X-ray diffraction. Yan et al. [30] used the corresponding stannylene to react with cesium fluoride to synthesize stable stannylene for the first time. Then Gross et al. [31] found that free stannylene can be obtained through stannylene. Subsequently, some experiments also investigated stannylene [32,33].

The reactions of silylenoids and germylenoids have been extensively studied such as the insertion reaction [34–50]. However, there are few theoretical research on the structure and reaction of stannylene. We think it is urgent to study the structure and reaction of stannylene theoretically, which is conducive to clarifying the reaction mechanism. In this work, we carry out systematic theoretical research on the insertion reaction of  $H_2SnLiF$  with  $NH_3$ ,  $H_2O$  and HF. We hope this work would supplement the reactivity of stannylene and provide a theoretical basis for the reaction of Sn-like compounds.

\* Correspondence: [liwenzuo2004@126.com](mailto:liwenzuo2004@126.com)

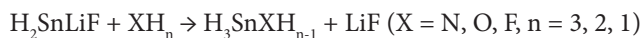
## 2. Theoretical methods

The M06-2X [51] methods with the def2-TZVP basis set were used to optimize the geometries of fixed points on the potential energy surface, and then the harmonic vibration frequency was calculated at the same level of theory to represent the minimum or first order saddle point of the optimized geometry. In order to improve the processing of electronic correlation, the QCISD [52] method was used to calculate the single point energy of all fixed points at the def2-TZVP theoretical level. The mechanism of the insertion reaction was verified by the analysis of the intrinsic reaction coordinate (IRC) of the possible transition state (TS). In order to consider the solvent effect, the SMD model [53] was used to calculate the geometry and energy of the fixed point in the insertion reaction, and tetrahydrofuran (THF) solvent was selected (dielectric constant  $\epsilon = 7.4257$ ). The Multiwfn and VMD softwares were used to draw frontier molecular orbitals [54–55]. All calculations were performed using the Gaussian 09 [56] series of programs.

## 3. Results and discussion

The previous work [57] has shown that when stannylene  $H_2Sn$ : and alkali halide LiF coexist, they are difficult to separate from each other and will exist in the form of stannyleneoid  $H_2SnLiF$ . The most stable configuration of  $H_2SnLiF$  at HF/3-21G level was found to be the p-complex configuration, followed by the three-membered ring configuration, and the energy barrier for the conversion between the two configurations is relatively large and difficult to convert. The M06-2X/def2-TZVP calculations in present work predicated similar results with Ref. [57]. There are three types of structures, namely p-complex configuration (RP), three-membered ring configuration (RS) and “classical” tetrahedral configuration for  $H_2SnLiF$ , which energies at the QCISD/def2-TZVP//M06-2X/def2-TZVP level are  $-322.1117$ ,  $-332.0977$  and  $-322.0687$  a.u., respectively. Therefore, the p-complex configuration and three-membered ring configuration are two basic structures of  $H_2SnLiF$ . On the other hand, the energy barrier for RP to RS is 111.96 kJ/mol, and the energy barrier for RS to RP is 75.62 kJ/mol, which means it is difficult to convert into each other for RP and RS. Therefore, in this work, we use the p-complex configuration (RP) and three-membered ring configuration (RP) to explore the insertion reaction with  $NH_3$ ,  $H_2O$ , and HF.

The insertion reaction of stannyleneoid  $H_2SnLiF$  with X-H bonds (X = N, O, F) can be described as the following equation:



Based on the calculated results, it can be reasonably predicted that the first step of the reaction between  $H_2SnLiF$  and  $XH_n$  is to form the precursor complex (Q). And there is a transition state (TS) and an intermediate (IM) along the reaction potential energy surface, and these structures connect reactants and products respectively. The Figure 1 shows the frontier molecular orbitals of p-complex configuration (RP) and three-membered ring configuration (RS) of  $H_2SnLiF$ . The Figures 2 and 3 show the reaction process and the relative energy and structural parameters of each stationary point of the potential energy surface (relative to the corresponding reactants). Figures 4 and 5 show changes in energy and bond distance of reaction coordinate of RP and RS with  $XH_n$  insertion reaction. Tables S1–S6 in Supporting information shows the charge changes of each atom in the insertion reaction of RP, RS with  $XH_n$ , respectively. Table S7 and S8 in Supporting information shows the energy of each stationary point on the potential energy surface of RP and RS insertion reaction.

### 3.1. Insertion reaction of p-complex configuration (RP)

The p-complex structure (RP) of  $H_2SnLiF$  can be regarded as a stannylene complex with ionic compound LiF (Figure 1). RP is formed by contributing some electrons of F atom in LiF to the unoccupied p orbital of Sn atom in singlet  $H_2Sn$ . In fact, there is also weak interaction between Li atom (with positive charge) and two H atoms (with negative charge). The highest occupied molecular orbital (HOMO) of RP is mainly composed of  $\sigma$  orbital on Sn atoms, so the RP shows obvious nucleophilicity in the  $\sigma$  orbital direction. The insertion reaction between RP and X-H bonds is caused by the interaction between the  $\sigma$  orbitals occupied by Sn atom and the s orbitals on H atoms of X-H bonds. When the H atom further approaches the Sn atom through the electrostatic interaction, the X end of the X-H bond also interacts with the Sn atom.

#### 3.1.1. The structures and energies of the precursor complexes

When  $XH_n$  is close to RP, the H end of X-H bonds and the  $\sigma$  orbital of Sn atom interaction forms precursor  $PQ_N$ ,  $PQ_O$ , and  $PQ_F$ . It can be seen from Figure 2 that the  $H_2SnLiF$  part of precursor  $PQ_N$ ,  $PQ_O$ , and  $PQ_F$  structure has little change compared with the reactant. The Sn-H distances are 3.297, 3.019, and 2.651 Å, and the distances of Sn-N, Sn-O and Sn-F are 2.708, 2.763, and 3.579 Å, respectively. The relative energies (shown in Figure 2) of  $PQ_N$ ,  $PQ_O$  and  $PQ_F$  are  $-29.39$ ,  $-17.01$ , and  $-15.75$  kJ/mol, respectively.

#### 3.1.2. The structures and energies of the transition states

As  $XH_n$  further approaches RP, the interaction between  $XH_{n-1}$  and the p orbital of Sn atom reaches the transition state  $RTSXH_n$ . As shown in Figure 2, the bond lengths of Sn- $H_a$ , Sn- $H_b$ , and Sn- $H_c$  are 2.810, 1.772, and 1.759 Å, and the

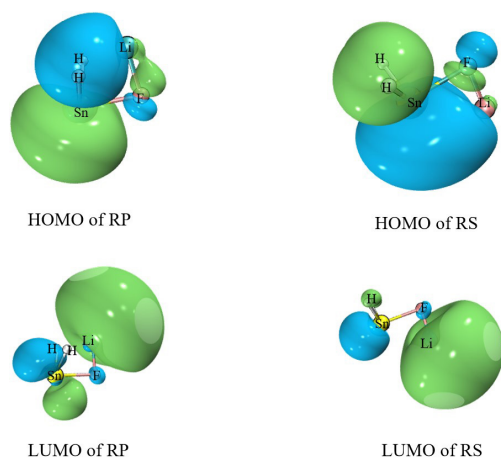


**Figure 1.** Frontier molecular orbitals of p-complex configuration (RP) and three-membered ring configuration (RS) of  $\text{H}_2\text{SnLiF}$  calculated at M06-2X/def2-TZVP level.

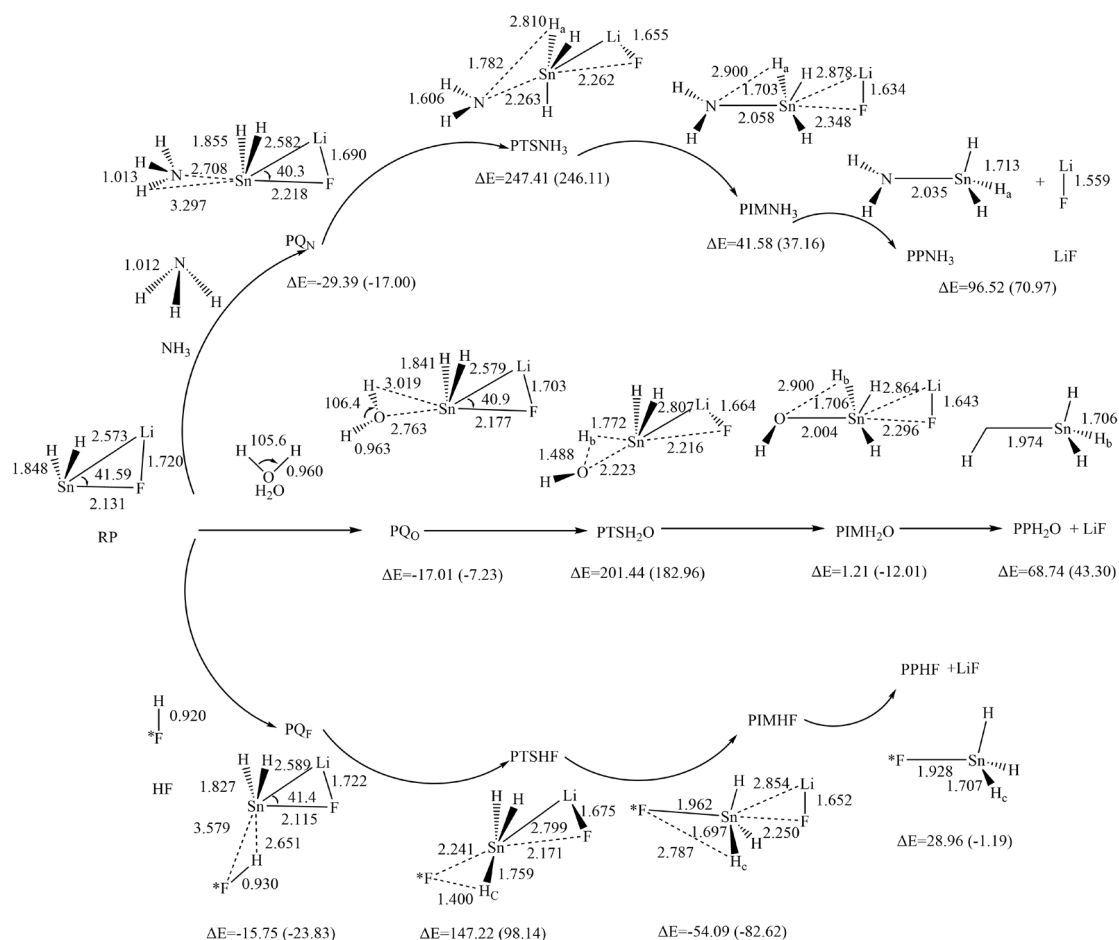


**Figure 2.** Schematic diagram of relative energy and structural parameters of each stationary point of the insertion reaction channel between RP and  $\text{NH}_3$ ,  $\text{H}_2\text{O}$  and  $\text{HF}$  and the reaction potential energy surface under the M06-2X method (the values in parentheses are the results obtained in THF solvent, bond length is in Å, bond angle is in degree).

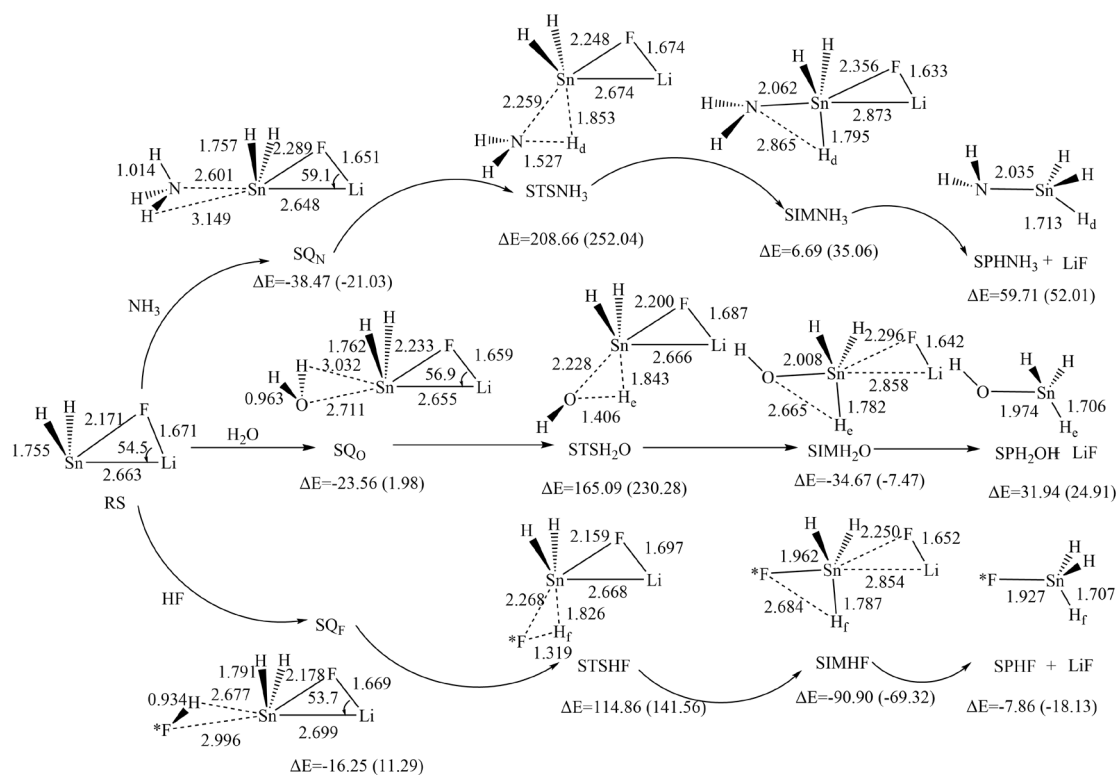


**Figure 3.** Schematic diagram of relative energy and structural parameters of each stationary point of the insertion reaction channel between RS and  $\text{NH}_3$ ,  $\text{H}_2\text{O}$  and HF and the reaction potential energy surface under the M06-2X method (the values in parentheses are the results obtained in THF solvent, bond length is in Å, bond angle is in degree).

distances of Sn-N, Sn-O and Sn-F are 2.263, 2.223, and 2.241 Å respectively. Compared with  $\text{PQ}_x$ , the bond lengths of Sn-H and Sn-X are significantly shorter. It can be seen from Tables S1–S3 in Supporting information that in this process, the natural charge of Sn atom increased from 1.438 to 2.242, 2.288, and 2.288, when X = N, O, F, respectively, and the natural charge of X and H atoms decreased significantly, which indicates that RP showed nucleophilic behavior in insertion reaction. Frequency analysis calculations performed at the M06-2X/def2-TZVP level of theory show that  $\text{PTSX}_n$  has a unique imaginary frequency (1413.7, 1438.8, 1393.9  $\text{cm}^{-1}$ ). IRC analysis shows that  $\text{PTSX}_n$  is the real transition state in the insertion reaction of  $\text{H}_2\text{SnLiF}$  with  $\text{XH}_n$ , and correctly connects the precursor complex  $\text{PQ}_x$  and the intermediate  $\text{PIMXH}_n$ . The relative energies of  $\text{PTSXH}_n$  are 247.41, 201.44, and 147.22 kJ/mol, when X = N, O, F, then the potential energy barrier of the insertion reaction are 276.80, 218.45, and 162.97 kJ/mol, respectively.

### 3.1.3. The structures and energies of the insertion intermediates

As the reaction proceeds, after  $\text{PTSXH}_n$ , the intermediate  $\text{PIMXH}_n$  is formed with the breaking of X-H bond and the generation of Sn-X and Sn-H bonds. In  $\text{PIMXH}_n$ , compared with  $\text{PTSXH}_n$ , the X-H bond was extended to 2.900, 2.900, and 2.787 Å, respectively, indicating that it was gradually broken during the formation of intermediates. The Sn-X and Sn-H distances were shortened to 2.058, 2.004, 1.962 and 1.703, 1.706, and 1.697 Å, respectively, indicating that the Sn-X and Sn-H bonds were gradually formed. While the Sn-F and Sn-Li bonds were significantly prolonged, indicating that the LiF part was gradually separated. At this time, the natural charge of the Sn atom increases, and the natural charge of X atom and H atom decreased significantly, indicating that the nucleophilic reaction continued to occur. The relative energies of  $\text{PIMXH}_n$  are 41.58, 1.21, and -54.09 kJ/mol, respectively.

### 3.1.4. The structures and energies of the products

As the reaction proceeds, when LiF is completely separated from Sn, the product  $\text{PPXH}_n$  is obtained. It can be found from Figure 2 that the structures of  $\text{PPNH}_3$ ,  $\text{PPH}_2\text{O}$  and  $\text{PPHF}$  are very similar, and they are all in four-coordinate configuration. Their relative energies are 96.52, 68.74, and 28.96 kJ/mol, respectively, indicating that the insertion reaction of RP is endothermic.

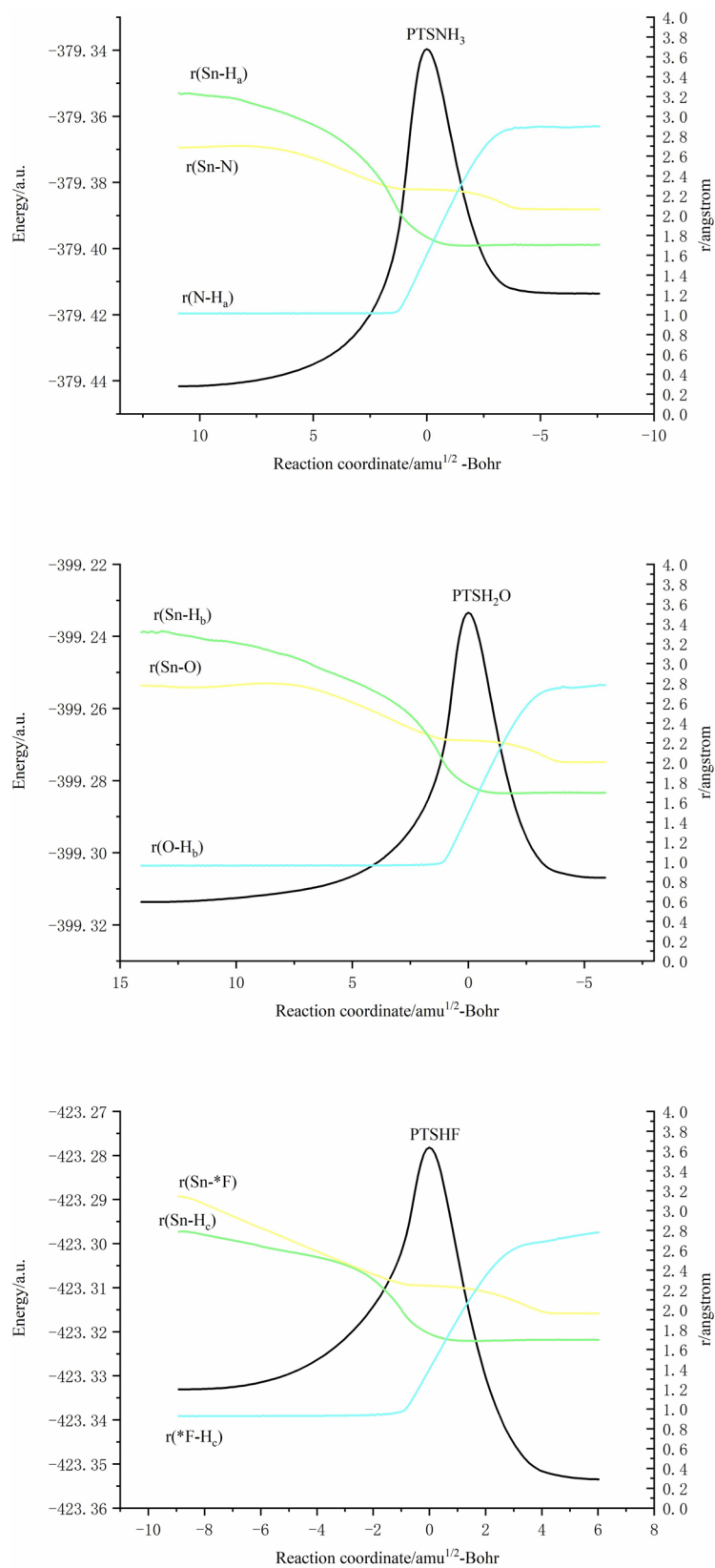


**Figure 4.** Changes in energy and bond distance of reaction coordinate of RP and  $\text{XH}_n$  ( $X = \text{N, O, F}$ ,  $n = 3, 2, 1$ ) insertion reaction.

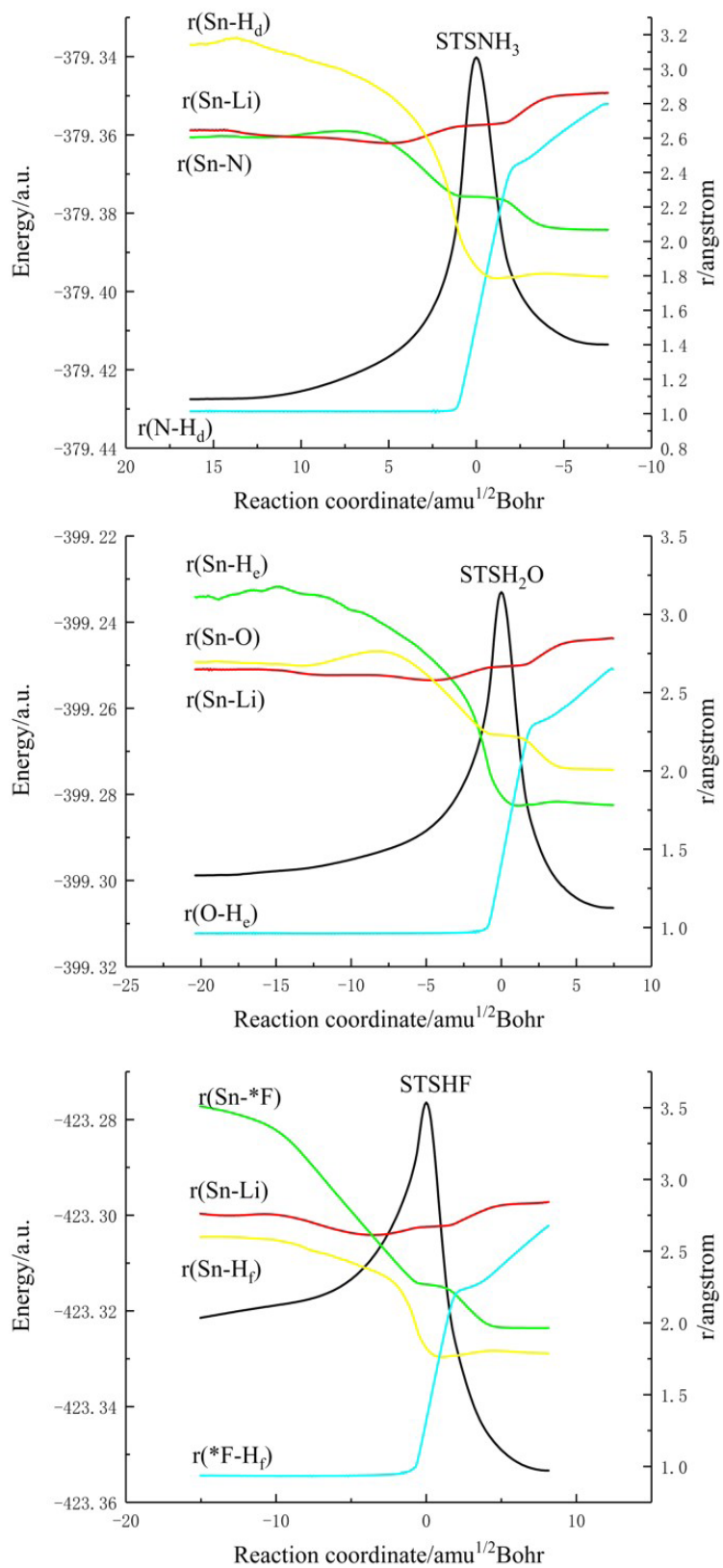


**Figure 5.** Changes in energy and bond distance of reaction coordinate of RS and  $\text{XH}_n$  ( $X = \text{N}, \text{O}, \text{F}$ ,  $n = 3, 2, 1$ ) insertion reaction.

As aforementioned, the insertion reaction of RP and  $XH_n$  is endothermic. The three products are similar. The order of the energy barrier is  $NH_3 > H_2O > HF$ , which indicates that HF is more prone to the insertion reaction, followed by  $H_2O$  and  $NH_3$ .

### 3.1.5. Mechanism of the insertion reaction

In order to explain the mechanism of the insertion reaction of RP with  $XH_n$ , we carried out the intrinsic reaction coordinate (IRC) analysis based on the optimized structure of transition states (PTSNH<sub>3</sub>, PTSH<sub>2</sub>O, PTSHF). Since the mechanism is similar, the reaction of RP with  $NH_3$  is chosen as an example to describe.

Figure 4 shows the changes of energy and Sn-H<sub>a</sub>, Sn-N and N-H<sub>a</sub> bond distances along the reaction coordinates. It can be seen from the figure that in the region of the reaction coordinate (10–0), the energy rises sharply and reaches the maximum energy at 0 point, which is in the transition state (PTSNH<sub>3</sub>). In this region, the distance between Sn-H<sub>a</sub> and Sn-N is continuously shortened, which means that  $NH_3$  is constantly approaching RP and has the tendency to form new bonds. The distance between N-H<sub>a</sub> bonds began to lengthen, and H<sub>a</sub> tended to leave  $NH_3$ . After 0 point, the energy of the reaction system begins to decrease. The distance between Sn-H<sub>a</sub> and Sn-N gradually decreases to a constant, which indicates that new Sn-H<sub>a</sub> and Sn-N bonds have been formed, accompanied by the fracture of N-H<sub>a</sub> bonds.

### 3.2. Insertion reaction of three-membered ring configuration (RS)

It can be seen from Figure 1 that the components of HOMO of RS are mainly concentrated on Sn atom and two H atoms, while the components of LUMO are mainly concentrated on Li atom, and a small part of them are concentrated on the p orbitals of Sn atom. Since the F atom gives electrons to the p orbital on the Sn atom, the p orbital on the Sn atom is not empty. When the insertion reaction occurs, the H end of the X-H bond first attacks the Sn atom  $\sigma$  orbit, and then close to RS, and the electron is partially transferred to the s orbital of H atom. Then, the X end of the X-H bond interacts with the p orbital on the Sn atom in RS to complete the reaction.

#### 3.2.1. The structures and energies of the precursor complexes

At the beginning of the reaction, X-H is close to RS, and the H end of X-H bond is connected with  $\sigma$  Orbital of Sn atom. The orbits combine to form the precursor  $SQ_x$ . From the Figure 3, the distances between Sn-X and Sn-H are 2.601, 2.711, 2.996 Å and 3.149, 3.032, 2.677 Å respectively, and the relative energies of  $SQ_N$ ,  $SQ_O$  and  $SQ_F$  are -38.47, -23.56, and -16.25 kJ/mol respectively, which indicates that this is an exothermic process.

#### 3.2.2. The structures and energies of the transition states

As  $XH_n$  approaches RS further, the X terminal interacts with the p orbital on the Sn atom on the back of the F atom in RS. The interaction between  $XH_n$  and Sn atom weakens the X-H bond. The reaction reached the transition state STSXH<sub>n</sub>. As shown in the Figure 3, the Sn-H distance was 1.853, 1.843, 1.826 Å and the Sn-X distance was 2.259, 2.228, and 2.268 Å respectively. Compared with  $SQ_x$ , the Sn-H and Sn-X distances were significantly shortened. It can be seen from the Tables (S4–S6) that the natural charge of sn atom increased from 1.522 to 2.305, 2.334, 2.317 respectively, and the natural charge of X and H atoms decreased significantly, indicating that this is a nucleophilic process. Frequency analysis calculations performed at the M06-2X/def2-TZVP level of theory show that STSX<sub>n</sub> has a unique imaginary frequency (1582.0, 1527.1, 1426.3 i cm<sup>-1</sup>). IRC analysis shows that STSX<sub>n</sub> is the real transition state in the insertion reaction of  $H_2SnLiF$  with  $XH_n$ , and correctly connects the precursor complex  $SQ_x$  and the intermediate SIMXH<sub>n</sub>. The relative energy of STSXH<sub>n</sub> is 208.66, 165.09, 114.86 kJ/mol respectively, so the potential barrier of RS insertion reaction is 247.13, 188.65, 131.11 kJ/mol respectively.

#### 3.2.3. The structures and energies of the insertion intermediates

After the transition state STSXH<sub>n</sub>, as the reaction proceeds, the X-H bond gradually breaks, the Sn-H and Sn-X bonds gradually form, forming the intermediate SIMXH<sub>n</sub>. At this time, the natural charge of the Sn atom increases, the natural charge of the X and H atoms decreases, the electrons of  $XH_n$  attack the Sn atom as a nucleophilic reagent, the ternary ring in RS is destroyed, the distance between the Li atom and the F atom is shortened, and there is a tendency to leave. The relative energy of SIMXH<sub>n</sub> is 6.69, -34.67 and -90.90 kJ/mol respectively.

#### 3.2.4. The structures and energies of the insertion products

As the reaction proceeds, LiF leaves and the product SPXH<sub>n</sub> is obtained. It can be seen from the Figure 3 that the structures of SPNH<sub>3</sub>, SPH<sub>2</sub>O and SPHF are very similar, and are the same as the insertion reaction products of RP. Their relative energies are 59.71, 31.94, and -7.86 kJ/mol respectively, indicating that the insertion reaction of RP with  $NH_3$  and  $H_2O$  is endothermic, and the reaction with HF is exothermic.

It can be seen from the above that the insertion reaction products of RS and  $XH_n$  are the same as those of RP reaction. The order of the insertion reaction barrier size is  $NH_3 > H_2O > HF$ , which is the same as that of RP reaction. And the reaction barrier of RS and RP are compared respectively. We find that the energy barrier overcome by RS is lower and the reaction is easier to occur.

### 3.2.4. Mechanism of the Insertion reaction

In order to explain the mechanism of the insertion reaction of RS with  $\text{NH}_3$ ,  $\text{H}_2\text{O}$  and HF, we carried out the intrinsic reaction coordinate (IRC) analysis based on the optimized structure of transition states ( $\text{STSNH}_3$ ,  $\text{STSH}_2\text{O}$ , and  $\text{STSHF}$ ). Taking the reaction with  $\text{NH}_3$  as an example, the reaction mechanism of RS and  $\text{XH}_n$  ( $X = \text{N}, \text{O}, \text{F}, n = 3, 2, 1$ ) will be summarized below.

Figure 5 shows the change of reaction coordinates along the reaction path of Sn- $\text{H}_d$ , Sn-N and N- $\text{H}_d$  distances with energy. In the reaction between RS and  $\text{NH}_3$ , it can be seen from the figure that in the region of the reaction coordinate (20–0), the energy rises sharply and reaches the maximum energy at point 0. At this time, it is in the transition state ( $\text{STSNH}_3$ ). In this region, we can see that the distance between Sn- $\text{H}_d$  and Sn-N is continuously shortened, which means that  $\text{NH}_3$  is constantly approaching RS, the distance between N- $\text{H}_d$  bonds begins to lengthen, and  $\text{H}_d$  has a tendency to leave  $\text{NH}_3$ . After 0, the energy of the system begins to decrease, and the system gradually becomes stable. The distance between Sn- $\text{H}_d$  and Sn-N is shortened to a certain extent and becomes stable, which indicates that new Sn- $\text{H}_d$  and Sn-N bonds have been formed. The distance between N- $\text{H}_d$  bonds is extended to a certain extent. At this time,  $\text{H}_d$  atom has been combined with Sn atom and LiF has been separated.

### 3.3. Solventing effect

In order to study the effect of solvent on the insertion reaction, we use the SMD model to set the insertion reaction to occur in THF solvent. The calculated results show that for the reaction involving RP, the inserted reaction barrier in THF solvent is 263.11, 190.19, 121.97 kJ/mol, which is lower than the reaction barrier in vacuum. For the reaction involving RS, the inserted reaction barrier in THF solvent is 273.07, 203.28, 141.56 kJ/mol, which is increased compared with the reaction barrier under vacuum. This shows that for RS, the reaction in THF solvent is unfavorable. For RP and RS, the order of difficulty of insertion reaction in THF solvent is  $\text{N} > \text{O} > \text{F}$ , and the reaction barrier of RS is lower than that of RP, so it is easier to conduct insertion reaction.

## 4. Conclusion

In this paper, the insertion reactions of the p-complex configuration (RP) and the ternary ring configuration (RS) of stannylene  $\text{H}_2\text{SnLiF}$  with  $\text{NH}_3$ ,  $\text{H}_2\text{O}$ , and HF have been studied theoretically. According to the calculation results, we know that the reaction products of RP and RS are the same, and through the calculation of the reaction energy barrier, the insertion reaction potential barrier of RS is lower than that of RP, which means that RS is easier to react. Comparing the reaction barrier of RP and RS with  $\text{NH}_3$ ,  $\text{H}_2\text{O}$ , and HF, we found that the difficulty of insertion reaction is  $\text{NH}_3 > \text{H}_2\text{O} > \text{HF}$ , regardless of the configuration of p-complex or three-membered ring. According to the calculation results, in THF solvent, the insertion reaction of RP with  $\text{NH}_3$ ,  $\text{H}_2\text{O}$ , and HF is favorable, while the insertion reaction of RS with  $\text{NH}_3$ ,  $\text{H}_2\text{O}$ , and HF is unfavorable. In addition, for RP and RS, the difficulty order of insertion reaction in THF solvent is  $\text{N} > \text{O} > \text{F}$ , and the reaction barrier of RS is lower than that of RP, so it is easier to conduct insertion reaction. We hope that the calculation results given in this paper are satisfactory and can make some useful predictions for the experiment.

## Acknowledgements

This research was supported by the National Natural Science Foundation Committee of China (No. 21103145), the Natural Science Foundation of Shandong Province (No. ZR2016BM23), and the Special Foundation of Youth Academic Backbone of Yantai University.

## References

- [1] Boche G, Lohrenz JCW. The electrophilic nature of carbenoids, nitrenoids, and oxenoids. *Chemical Reviews* 2001; 101 (3): 697-756. <https://doi.org/10.1021/cr940260x>
- [2] Rappoport, Z, Marek I. The chemistry of organolithium compounds. 2004; John Wiley & Sons. <https://doi.org/10.1002/047002111X>
- [3] Nozakura S, Konotsune S. Cyanoethylation of Trichlorosilane. I.  $\beta$ -Addition. *Bulletin of the Chemical Society of Japan* 1956; 29 (3): 322-326. <https://doi.org/10.1246/bcsj.29.322>
- [4] Zon G, DeBruin KE, Naumann K, Mislou K. Stereospecific desulfurization of acyclic phosphine sulfides with hexachlorodisilane and the alkaline hydrolysis of monoalkoxy- and monoalkylthiophosphonium salts. *Journal of the American Chemical Society* 1969; 91 (25): 7023-7027. <https://doi.org/10.1021/ja01053a022>

- [5] Oehme H, Weiss H. Reaction of 2,4,6-tri-*t*-butylphenyllithium with bromotrichlorosilane. Generation of trichlorosilyllithium, LiSiCl<sub>3</sub>. *Journal of Organometallic Chemistry* 1987; 319 (1): C16-C18. [https://doi.org/10.1016/0022-328X\(87\)80359-5](https://doi.org/10.1016/0022-328X(87)80359-5)
- [6] Kawachi A, Tamao K. Preparations and reactions of functionalized silyllithiums. *Bulletin of the Chemical Society of Japan* 1997; 70 (5): 945-955. <https://doi.org/10.1246/bcsj.70.945>
- [7] Tamao K, Kawachi A, Asahara M, Toshimitsu A. Recent developments in silicon interelement linkage: the case of functionalized silyllithium, silylenoid and sila-ylide. *Pure and Applied Chemistry* 1999; 71 (3): 393-400. <https://doi.org/10.1351/pac199971030393>
- [8] Tokitoh N, Hatano K, Sadahiro T, Okazaki R. Generation and reactions of an overcrowded diaryldilithiosilane. *Chemistry letters* 1999; 28 (9): 931-932. <https://doi.org/10.1246/cl.1999.931>
- [9] Kawachi A, Tamao K. Structures of [(Amino) phenylsilyl] lithiums and Related Compounds in Solution and in the Solid State. *Journal of the American Chemical Society* 2000; 122 (9): 1919-1926. <https://doi.org/10.1021/ja993101+>
- [10] Fischer R, Baumgartner J, Kickelbick G, Marschner C. The first stable  $\beta$ -fluorosilylanion. *Journal of the American Chemical Society* 2003; 125 (12): 3414-3415. <https://doi.org/10.1021/ja0291639>
- [11] Lee ME, Cho HM, Lim YM, Choi JK, Park CH et al. Syntheses and reactivities of stable halosilylenoids, (Tsi)X<sub>2</sub>SiLi (Tsi = C(SiMe<sub>3</sub>)<sub>3</sub>, X = Br, Cl). *Chemistry—A European Journal* 2004; 10 (2): 377-381. <https://doi.org/10.1002/chem.200305151>
- [12] Molev G, Bravo-Zhivotovskii D, Karni M, Tumanskii B, Botoshansky M et al. Synthesis, molecular structure, and reactivity of the isolable silylenoid with a tricoordinate silicon. *Journal of the American Chemical Society* 2006; 128 (9): 2784-2785. <https://doi.org/10.1021/ja0575880>
- [13] Cho HM, Lim YM, Lee ME. Reactivities of chlorotrisylsilylenoid with ketones. *Dalton Transactions* 2010; 39 (39): 9232-9234. <https://doi.org/10.1039/C0DT00147C>
- [14] Lim YM, Park CH, Yoon SJ, Cho HM, Lee ME et al. New synthetic routes for silaheterocycles: reactions of a chlorosilylenoid with aldehydes. *Organometallics* 2010; 29 (6): 1355-1361. <https://doi.org/10.1021/om9008789>
- [15] Cho HM, Bok K, Park SH, Lim YM, Lee ME et al. A new synthetic route for silacyclopropanes: reactions of a bromosilylenoid with olefins. *Organometallics* 2012; 31 (15): 5227-5230. <https://doi.org/10.1021/om3005349>
- [16] Clark T, Schleyer P von R. The isomeric structures of SiH<sub>2</sub>LiF. *Journal of Organometallic Chemistry* 1980; 191 (2): 347-353. [https://doi.org/10.1016/S0022-328X\(00\)81063-3](https://doi.org/10.1016/S0022-328X(00)81063-3)
- [17] Qi Y, Ma J, Xu C, Geng B, He M. Computational investigations on the electronic and structural properties of the unsaturated silylenoid HP=SiLiF. *Journal of Molecular Modeling* 2014; 20: 1-6. <https://doi.org/10.1007/s00894-014-2213-9>
- [18] Yildiz CB, Azizoglu A. A mechanistic investigation on the formation and rearrangement of silaspiropentane: a theoretical study. *Journal of Molecular Modeling* 2016; 22: 1-7. <https://doi.org/10.1007/s00894-016-3016-y>
- [19] Suzuki Y, Sasamori T, Guo JD, Nagase S, Tokitoh N. Frontispiece: Isolation and Ambident Reactivity of a Chlorogermolenoid. *Chemistry—A European Journal* 2016; 22 (39). <https://doi.org/10.1002/chem.201683961>
- [20] Ma WY, Zhu YF, Zhou JH, Fang YZ. Solvent effect on the structures and isomerization of germolenoid GeH<sub>2</sub>LiF. *Journal of Molecular Structure: THEOCHEM* 2007; 817 (1-3): 77-81. <https://doi.org/10.1016/j.theochem.2007.04.023>
- [21] Li WZ, Gong BA, Cheng JB, Xiao CP. Theoretical study on the beryllium chlorogermolenoid H<sub>2</sub>GeClBeC. *Journal of Molecular Structure: THEOCHEM* 2007; 847 (1-3): 75-78. <https://doi.org/10.1016/j.theochem.2007.08.036>
- [22] Li WZ, Cheng JB, Li QZ, Gong BA, Sun JZ. Theoretical investigation on structures and isomerizations of the aluminum chlorogermolenoid H<sub>2</sub>GeClAlCl<sub>2</sub>. *Journal of Organometallic Chemistry* 2009; 694 (18): 2898-2901. <https://doi.org/10.1016/j.jorganchem.2009.04.023>
- [23] Tanaka Y, Hada M, Kawachi A, Tamao K, Nakatsuji H. Self-Condensation Reaction of Lithium (Alkoxy) silylenoid: A Model Study by ab Initio Calculation. *Organometallics* 1998; 17 (21): 4573-4577. <https://doi.org/10.1021/om980567c>
- [24] Song JH, Park SH, Cho HM, Lee ME. Reactivity of bromosilylenoid with heterocumulenes. *Journal of Organometallic Chemistry* 2015; 799: 128-131. <https://doi.org/10.1016/j.jorganchem.2015.09.016>
- [25] Ohtaki T, Ando W. Dichlorodigermacyclobutanes and Digermabicyclo [2.2.0] hexanes from the Reactions of [Tris (trimethylsilyl) methyl] chlorogermylene with Olefins. *Organometallics* 1996; 15 (14): 3103-3105. <https://doi.org/10.1021/om9600147>
- [26] Filippou AC, Stumpf KW, Chernov O, Schnakenburg G. Metal Activation of a Germolenoid, a New Approach to Metal–Germanium Triple Bonds: Synthesis and Reactions of the Germolydine Complexes [Cp(CO)<sub>2</sub>MGe–C(SiMe<sub>3</sub>)<sub>3</sub>](M = Mo, W). *Organometallics* 2012; 31 (2): 748-755. <https://doi.org/10.1021/om201176n>
- [27] Grugel C, Neumann WP, Sauer J, Seifert P. A highly stereoselective C-C coupling of aldehydes forming glycols via a stannyleneid reaction. *Tetrahedron Letters* 1978; 19 (31): 2847-2850. [https://doi.org/10.1016/S0040-4039\(01\)94880-4](https://doi.org/10.1016/S0040-4039(01)94880-4)
- [28] Arif AM, Cowley AH, Elkins TM. A bulky silyl derivative of tin (II). *Journal of Organometallic Chemistry* 1987; 325 (1-2): C11-C13. [https://doi.org/10.1016/0022-328X\(87\)80413-8](https://doi.org/10.1016/0022-328X(87)80413-8)

- [29] Ochiai T, Franz D, Wu XN, Irran E, Inoue S. A Tin Analogue of Carbenoid: Isolation and Reactivity of a Lithium Bis (imidazolin-2-imino) stannylene. *Angewandte Chemie International Edition* 2016; 55 (24): 6983-6987. <https://doi.org/10.1002/anie.201602178>
- [30] Yan C, Li Z, Xiao X Q, Wei N, Lu Q et al. Reversible Stannylene Formation from the Corresponding Stannylene and Cesium Fluoride. *Angewandte Chemie International Edition* 2016; 55 (47): 14784-14787. <https://doi.org/10.1002/anie.201608162>
- [31] Gross LW, Moser R, Neumann WP, Scherping K H. Insertion reactions of thermally generated stannylenes R<sub>2</sub>Sn into Sn-X (X = Cl, Br, SPh) and Sn-Sn bonds. *Tetrahedron Letters* 1982; 23 (6): 635-638. [https://doi.org/10.1016/S0040-4039\(00\)86909-9](https://doi.org/10.1016/S0040-4039(00)86909-9)
- [32] Fu J, Neumann WP. Organozinnverbindungen: XXX. Über das hexa-9-phenantryl-cyclostristanan. *Journal of Organometallic Chemistry* 1984; 272 (1): C5-C9. [https://doi.org/10.1016/0022-328X\(84\)80448-9](https://doi.org/10.1016/0022-328X(84)80448-9) (in German).
- [33] Klinkhammer K. Dihypersilylstannylene and dihypersilylplumbylene—two Lewis-amphoteric carbene homologues. *Polyhedron* 2002; 21 (5-6): 587-598. [https://doi.org/10.1016/S0277-5387\(01\)01029-4](https://doi.org/10.1016/S0277-5387(01)01029-4)
- [34] Xie J, Feng D, Feng S, Zhang J. Theoretical study on the reaction of silylenoid H<sub>2</sub>SiLiF with HF. *Chemical Physics* 2006; 323 (2-3): 185-192. <https://doi.org/10.1016/j.chemphys.2005.08.053>
- [35] Xie J, Feng D, Feng S. Insertion of the p-complex structure of silylenoid H<sub>2</sub>SiLiF into X-H bonds (X = C, Si, N, P, O, S, and F). *Journal of Organometallic Chemistry* 2006; 691 (1-2): 208-223. <https://doi.org/10.1016/j.jorganchem.2005.08.031>
- [36] Qi Y, Feng D, Li R, Feng S. Theoretical study on the substitution and insertion reactions of silylenoid H<sub>2</sub>SiLiF with CH<sub>3</sub>XHn-1 (X = F, Cl, Br, O, N; n = 1, 1, 1, 2, 3). *Journal of Organometallic Chemistry* 2009; 694 (5): 771-779. <https://doi.org/10.1016/j.jorganchem.2008.12.017>
- [37] Li WZ, Yan BF, Xiao CP, Li QZ, Cheng JB. Novel formation of silicon-germanium bond: Insertion reactions of H<sub>2</sub>SiLiF with GeH<sub>3</sub>X (X = F, Cl, Br). *Journal of Organometallic Chemistry* 2014; 750: 112-116. <https://doi.org/10.1016/j.jorganchem.2013.11.018>
- [38] Xie J, Feng D, Feng S, Zhang J. Theoretical study on insertion of silylenoid H<sub>2</sub>SiLiF into X-H bonds (X = CH<sub>3</sub>, SiH<sub>3</sub>, NH<sub>2</sub>, PH<sub>2</sub>, OH, SH and F). *Journal of Molecular Structure: THEOCHEM* 2005; 755 (1-3): 55-63. <https://doi.org/10.1016/j.theochem.2005.07.027>
- [39] Xie J, Feng D, He M, Feng S. Insertion Reactions of Silylenoid Ph<sub>2</sub>SiLi (OBU-t) into X-H Bonds (X = F, OH, and NH<sub>2</sub>). *The Journal of Physical Chemistry A* 2005; 109 (46): 10563-10570. <https://doi.org/10.1021/jp053290k>
- [40] Feng S, Feng D, Li J. An ab initio study on the insertion reaction of silylenoid H<sub>2</sub>SiLiF with H<sub>2</sub>. *Chemical Physics Letters* 2000; 316 (1-2): 146-150. [https://doi.org/10.1016/S0009-2614\(99\)01269-5](https://doi.org/10.1016/S0009-2614(99)01269-5)
- [41] Qi Y, Geng B, Chen Z. The insertion reactions of the p-complex silylenoid H<sub>2</sub> SiLiF with Si-X (X = F, Cl, Br, O, N) bonds. *Journal of Molecular Modeling* 2012; 18: 1015-1021. <https://doi.org/10.1007/s00894-011-1129-x>
- [42] Tan X, Wang W, Li P, Wang Q, Zheng G et al. Theoretical studies on the imine germylenoid HNGeNaF and its insertion reaction with R-H (R = F, OH, NH<sub>2</sub>, CH<sub>3</sub>). *Journal of Organometallic Chemistry* 2008; 693 (3): 475-482. <https://doi.org/10.1016/j.jorganchem.2007.11.019>
- [43] Li WZ, Yan BF, Li QZ, Cheng JB. The insertion reactions of the germylenoid H<sub>2</sub>GeLiF with CH<sub>3</sub>X (X = F, Cl, Br). *Journal of Organometallic Chemistry* 2013; 724: 163-166. <https://doi.org/10.1016/j.jorganchem.2012.11.012>
- [44] Yan BF, Li WZ, Pei YW, Li QZ, Cheng JB. Theoretical investigation on the insertion reactions of the germylenoid H<sub>2</sub>GeLiF with RH (R = Cl, SH, PH<sub>2</sub>). *Journal of Theoretical and Computational Chemistry* 2013; 12 (03): 1350003. <https://doi.org/10.1142/S021963361350003X>
- [45] Yan BF, Li WZ, Xiao CP, Liu ZB, Li QZ et al. New insights into the insertion reactions of germylenoid H<sub>2</sub>GeLiF with RH (R = F, OH, NH<sub>2</sub>). *Journal of Molecular Modeling* 2015; 21: 1-6. <https://doi.org/10.1007/s00894-015-2626-0>
- [46] Tan X, Wang W, Li P, Liu F. Theoretical studies on the alkylidene germylenoid H<sub>2</sub>C=GeLiF and its insertion reaction with RH (R = F, OH, NH<sub>2</sub>, CH<sub>3</sub>). *Russian Journal of Physical Chemistry A* 2009; 83: 1355-1362. <https://doi.org/10.1134/S0036024409080184>
- [47] Li WZ, Pei YW, Cheng JB, Li QZ, Gong BA. Theoretical study on the insertion reactions of the germylenoid H<sub>2</sub>GeClMgCl with RH (R = F, OH, NH<sub>2</sub>). *Russian Journal of Physical Chemistry A* 2012; 86: 1969-1973. <https://doi.org/10.1134/S0036024412130225>
- [48] Zhang MX, Xiao CP, Liu ZB, Li WZ, Li QZ et al. Theoretical prediction on the insertion reactions of the germylenoid H<sub>2</sub>GeLiF with GeH<sub>3</sub>X (X = F, Cl, Br). *Russian Journal of Physical Chemistry A* 2015; 89: 1872-1877. <https://doi.org/10.1134/S0036024415100234>
- [49] Zhang MX, Yan BF, Li WZ, Li QZ, Cheng JB. The insertion and H<sub>2</sub> elimination reactions of H<sub>2</sub>GeFMgF germylenoid with RH (R = Cl, SH, PH<sub>2</sub>). *Russian Journal of Physical Chemistry A* 2017; 91: 1660-1668. <https://doi.org/10.1134/S0036024417090205>
- [50] Zhang MX, Zhang MJ, Li WZ, Li QZ, Cheng JB. Structure of H<sub>2</sub>GeFMgF and its insertion reactions with RH (R = F, OH, NH<sub>2</sub>). *Journal of Theoretical and Computational Chemistry* 2015; 14 (01): 1550004. <https://doi.org/10.1142/S0219633615500042>
- [51] Hohenstein EG, Chill ST, Sherrill CD. Assessment of the performance of the M05-2X and M06-2X exchange-correlation functionals for noncovalent interactions in biomolecules. *Journal of Chemical Theory and Computation* 2008; 4 (12): 1996-2000. <https://doi.org/10.1021/ct800308k>
- [52] Gauss J, Cremer D. Analytical evaluation of energy gradients in quadratic configuration interaction theory. *Chemical Physics Letters* 1988; 150 (3-4): 280-286. [https://doi.org/10.1016/0009-2614\(88\)80042-3](https://doi.org/10.1016/0009-2614(88)80042-3)

- [53] Marenich AV, Cramer CJ, Truhlar DG. Performance of SM6, SM8, and SMD on the SAMPL1 test set for the prediction of small-molecule solvation free energies. *The Journal of Physical Chemistry B* 2009; 113 (14): 4538-4543. <https://doi.org/10.1021/jp809094y>
- [54] Humphrey W, Dalke A, Schulten K. VMD: visual molecular dynamics. *Journal of molecular graphics* 1996; 14 (1): 33-38. [https://doi.org/10.1016/0263-7855\(96\)00018-5](https://doi.org/10.1016/0263-7855(96)00018-5)
- [55] Lu T, Chen F. Multiwfn: A multifunctional wavefunction analyzer. *Journal of Computational Chemistry* 2012; 33 (5): 580-592. <https://doi.org/10.1002/jcc.22885>
- [56] Frisch MJ, Trucks GW, Schlegel HB, Scuseria GE, Robb MA et al. Gaussian 09, revision A02. Gaussian Inc, Wallingford, CT, 2009.
- [57] Qiu HY, Deng CH. Theoretical studies on the structures and reactivity of stannyleneoids I. The structures and isomerization of stannyleneoid H<sub>2</sub>SnLiF. *Chinese Journal of Chemistry* 1996; 14 (4): 310-314. <https://doi.org/10.1002/cjoc.19960140405>

## Supporting information

**Table S1.** Natural bond orbital analysis (NBO) of the stagnation points on the potential energy surface of RP and NH<sub>3</sub> insertion reaction at M06-2X/def2-TZVP level.

Structure	Sn	F	Li	H	H	N	H <sub>a</sub>	H <sub>N1</sub>	H <sub>N2</sub>
RP	1.438	-0.884	0.764	-0.659	-0.659				
NH <sub>3</sub>						-1.053	0.351	0.351	0.351
LiF		0.923	-0.923						
PTSNH <sub>3</sub>	2.242	-0.900	0.861	-0.577	-0.687	-1.446	-0.215	0.363	0.358
PIMNH <sub>3</sub>	2.696	-0.907	0.875	-0.571	-0.682	-1.554	-0.571	0.361	0.361
PPNH <sub>3</sub>	2.554			-0.581	-0.581	-1.538	-0.592	0.369	0.369

(Tips: H<sub>N1</sub> and H<sub>N2</sub> are atoms connected with N atom).**Table S2.** Natural bond orbital analysis (NBO) of the stagnation points on the potential energy surface of RS and H<sub>2</sub>O insertion reaction at M06-2X/def2-TZVP level.

Structure	Sn	F	Li	H	H	O	H <sub>b</sub>	H <sub>o</sub>
RP	1.438	-0.884	0.764	-0.659	-0.659			
H <sub>2</sub> O						-0.919	0.459	0.459
LiF		0.923	-0.923					
PTSH <sub>2</sub> O	2.288	-0.899	0.869	-0.589	-0.683	-1.257	-0.198	0.469
PIMH <sub>2</sub> O	2.724	-0.907	0.883	-0.582	-0.688	-1.319	-0.569	0.460
PPH <sub>2</sub> O	2.589			-0.589	-0.589	-1.302	-0.577	0.470

(Tips: H<sub>o</sub> are atoms connected with O atom).**Table S3.** Natural bond orbital analysis (NBO) of the stagnation points on the potential energy surface of RP and HF insertion reaction at M06-2X/def2-TZVP level.

Structure	Sn	F	Li	H	H	*F	H <sub>f</sub>
RP	1.438	-0.884	0.764	-0.659	-0.659		
HF						-0.550	0.550
LiF		0.923	-0.923				
PTSHF	2.288	-0.898	0.877	-0.685	-0.579	-0.812	-0.190
PIMHF	2.732	-0.907	0.890	-0.575	-0.575	-0.881	-0.684
PPHF	2.603			-0.581	-0.581	-0.859	-0.582

(Tips: H<sub>f</sub> are atoms connected with \*F atom).**Table S4.** Natural bond orbital analysis (NBO) of the stagnation points on the potential energy surface of RS and NH<sub>3</sub> insertion reaction at M06-2X/def2-TZVP level.

Structure	Sn	F	Li	H	H	N	H <sub>d</sub>	H <sub>N1</sub>	H <sub>N2</sub>
RS	1.522	-0.894	0.588	-0.608	-0.608				
NH <sub>3</sub>						-1.053	0.351	0.351	0.351
LiF		0.923	-0.923						
STSNH <sub>3</sub>	2.305	-0.897	0.676	-0.574	-0.574	-1.454	-0.220	0.368	0.371
SIMNH <sub>3</sub>	2.694	-0.907	0.880	-0.578	-0.574	-1.561	-0.680	0.362	0.364
SPNH <sub>3</sub>	2.554			-0.581	-0.581	-1.538	-0.592	0.369	0.369

(Tips: H<sub>N1</sub> and H<sub>N2</sub> are atoms connected with N atom).

**Table S5.** Natural bond orbital analysis (NBO) of the stagnation points on the potential energy surface of RS and H<sub>2</sub>O insertion reaction at M06-2X/def2-TZVP level.

Structure	Sn	F	Li	H	H	O	H <sub>c</sub>	H <sub>o</sub>
RS	1.522	-0.894	0.588	-0.608	-0.608			
H <sub>2</sub> O						-0.919	0.459	0.459
LiF		0.923	-0.923					
STSH <sub>2</sub> O	2.334	-0.896	0.692	-0.583	-0.571	-1.245	-0.201	0.472
SIMH <sub>2</sub> O	2.723	-0.907	0.887	-0.582	-0.582	-1.321	-0.678	0.460
SPH <sub>2</sub> O	2.589			-0.590	-0.590	-1.302	-0.577	0.470

(Tips: H<sub>o</sub> are atoms connected with O atom).**Table S6.** Natural bond orbital analysis (NBO) of the stagnation points on the potential energy surface of RS and HF insertion reaction at M06-2X/def2-TZVP level.

Structure	Sn	F	Li	H	H	*F	H <sub>f</sub>
RS	1.522	-0.894	0.588	-0.608	-0.608		
HF						-0.550	0.550
LiF		0.923	-0.923				
STSHF	2.317	-0.897	0.722	-0.572	-0.572	-0.803	-0.194
SIMHF	2.732	-0.907	0.890	-0.575	-0.575	-0.881	-0.684
SPHF	2.603			-0.581	-0.581	-0.859	-0.582

(Tips: H<sub>f</sub> are atoms connected with \*F atom).**Table S7.** Energy of each stationary point on the potential energy surface of RP insertion reaction (kJ/mol).

Structure	Energy (vacuum)/a.u.	Energy (THF)/a.u.
RP	-322.1117	-322.1550
NH <sub>3</sub>	-56.4575	-56.4621
H <sub>2</sub> O	-76.3200	-76.3262
HF	-100.3336	-100.3385
QPNH <sub>3</sub>	-378.5805	-378.6236
QPH <sub>2</sub> O	-398.4382	-398.4839
OPHF	-422.4513	-422.5025
TSPNH <sub>3</sub>	-378.4751	-378.5233
TSPH <sub>2</sub> O	-398.3550	-398.4115
TSPHF	-422.3892	-422.4560
IMPNH <sub>3</sub>	-378.5535	-378.6029
IMPH <sub>2</sub> O	-398.4313	-398.4857
IMPHF	-422.4659	-422.5249
PPNH <sub>3</sub>	-271.2763	-271.2805
PPH <sub>2</sub> O	-291.1493	-291.1551
PPHF	-315.1780	-315.1843
LiF	-107.2563	-107.3095

**Table S8.** Energy of each stationary point on the potential energy surface of RS insertion reaction (kJ/mol).

Structure	Energy (vacuum)/a.u.	Energy (THF)/a.u.
RS	-322.0977	-322.1262
QSNH <sub>3</sub>	-378.5699	-378.5966
QSH <sub>2</sub> O	-398.4267	-398.4522
OSHF	-422.4375	-422.4629
TSSNH <sub>3</sub>	-378.4758	-378.4925
TSSH <sub>2</sub> O	-398.3549	-398.3755
TSSHF	-422.3875	-422.4133
IMSNH <sub>3</sub>	-378.5527	-378.5752
IMSH <sub>2</sub> O	-398.4309	-398.4558
IMSHF	-422.4659	-422.4936
PSNH <sub>3</sub>	-271.2763	-271.2796
PSH <sub>2</sub> O	-291.1493	-291.1543
PSHF	-315.1780	-315.1850